Prediction of the Stamped Part Thinning Depending on Its Geometry and Blank Material

Jan Řiháček, Kamil Podaný, František Faltýnek

Institute of Manufacturing Technology, Faculty of Mechanical Engineering, Brno University of Technology. Technická 2896/2, 616 69 Brno. Czech Republic. E-mail: rihacek.j@fme.vutbr.cz, podany@fme.vutbr.cz, 152489@vutbr.cz

The paper deals with a design of new dimple geometry with a view to minimizing its thinning. In this case, three types of blank materials were analyzed, i.e. ferritic steel X2CrCuTi18, austenitic steel X5CrNi18-10 and austenitic steel X5CrNi18-10 with additional heat treatment. Thinning analysis for different dimple geometry and blank material is performed with a numerical simulation using finite element method in ANSYS software. To verify the accuracy of the numerical simulation, a practical stamping of the part with initial design and comparison between resulting thinning values, which is determined by ANSYS software and experimental microscopic measurement, is also performed.

Keywords: Numerical Simulation, Forming, Dimple, ANSYS, Finite Element Method

1 Introduction

In the most cases, the creation of shallow dimples in a sheet metal part is intended to increase its stiffness. In general, it is an unsymmetrical bending to a non-expandable shape, most often in the shape of grooves, wherein the dimples may be of substantially any shape. [1], [2] The article is aimed at optimization of the circular dimples geometry on the stamped part (Fig. 1) in the application for the automotive industry. Production of the optimized component is carried out at Hanon Systems Autopal company, which belongs to the Hanon Systems concern. The company is in the automotive industry focusing on systems that regulate both the temperature inside the car cabin and the engine temperature.

With regard to the confidentiality, only approximate dimensions of the optimized part are given. Mentioned dimples here primarily do not increase the stiffness of the whole part, but they serve primarily as a spacer to which another part is soldered, see the detail of the soldered joint in Fig. 2. When a thermal load is applied on this assembly, during operating load, cracks occur in areas with the most thinning. Therefore, the main aim is to optimize the dimples shape with the simultaneous analysis of the blank material to obtain the smallest dimple thinning in transitions between the dimple and a flat region of the stamped part. [3]
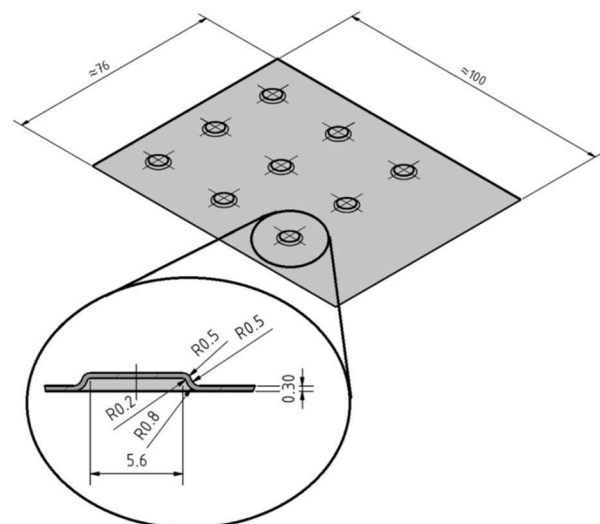

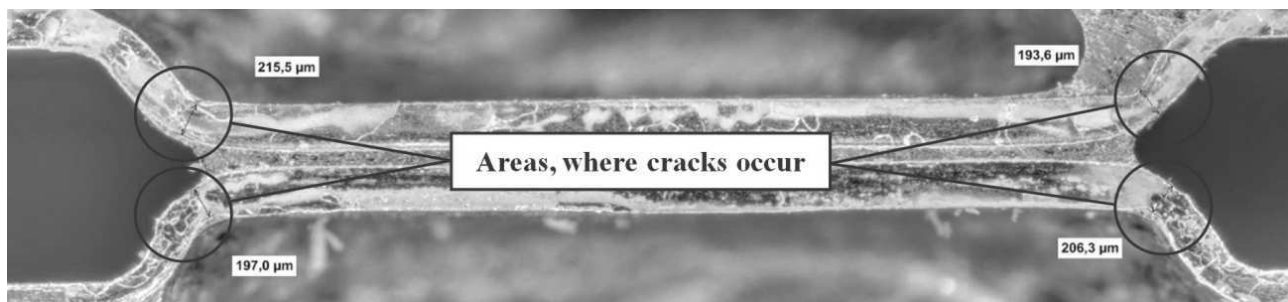**Fig. 1** *Basic Dimensions of the Optimized Part*

Fig. 2 *Crosssection of Two Soldered Dimples [3]*

The current initial blank for the production of the mentioned part is a 0.3 mm thick sheet, which is made of X2CrCuTi18 steel. It is stainless ferritic steel with chemical composition, which is shown in Tab. 1. Basic mechanical and physical properties, which are for 20 °C defined by the standard, are also mentioned in Tab. 2.

Tab. 1 *Chemical Composition of X2CrCuTi18 Steel [3]*

	C	Mn	P	S	Si	Cr	Cu	Ti	N
min.	-	-	-	-	-	16.000	0.300	-	-
max.	0.025	1.000	0.040	0.030	1.000	20.000	0.800	0.800	0.250

Tab. 2 *Basic Mechanical and Physical Properties of X2CrCuTi18 Steel [3]*

Yield Stress	Ultimate Strength	Ductility	Young's modulus	Poisson's Ratio	Density
$R_{p0.2}$ [MPa]	R_m [MPa]	A_{80} [%]	E [GPa]	μ [-]	ρ [kg·m^{-3}]
205	390	22	195	0.31	7700

Another considered material variant is a sheet of the same thickness of X5CrNi18-10 steel, which, due to 10% nickel presence, ranks among austenitic stainless steels. [4] The contents of all alloying elements are shown in Tab. 3. Compared to the previous material, mechanical properties are characterized by low yield strength and high ductility, see Tab. 4.

Tab. 3 *Chemical Composition of X5CrNi18-10 Steel [6]*

|	C	Mn	P	S	Si	Ni	Cr	N
min.	-	-	-	-	-	8.000	17.000	-
max.	0.070	2.000	0.045	0.030	1.000	10.500	20.000	0.100

Tab. 4 *Basic Mechanical and Physical Properties of X5CrNi18-10 Steel [6]*

Yield Stress	Ultimate Strength	Ductility	Young's modulus	Poisson's Ratio	Density
$R_{p0.2}$ [MPa]	R_m [MPa]	A_{80} [%]	E [GPa]	μ [-]	ρ [kg·m^{-3}]
190	500 ÷ 750	37	199	0.3	8030

As a standard for this type of steel, dissolving annealing is carried out in which austenite is homogenized followed by rapid cooling. This procedure prevents local decrease of the chromium concentration and loss of resistance to intergranular corrosion. [4], [5] Moreover, additional heat treatment – annealing can be carried out, that further improves the steel structure and its properties. The temperature of 1 040 °C is reached by the initial heating. After 3 minutes at constant temperature, the step heating is continued at 1 060 °C, 1 070 °C and 1 080 °C, always with the same delay. The heating process is followed by free air cooling to ambient temperature. It is important to note, that for the production of the desired part, X5CrNi18-10 steel was available both after standard annealing and after additional annealing.

## 2 Analysis of the Current State

Firstly, it is necessary to measure the thinning of the critical areas on actual stamped parts with dimples. This means to measure thinning of parts that were made of X2CrCuTi18 steel. The SSM-3E microscope, which is equipped with a USB camera, was used to perform wall thickness measurements on manufactured parts with support of Dino-Capture 2.0 software. Overall, two stamped parts were cut into longitudinal and transverse sections taken through the dimples, as it is schematically shown in Fig. 3. The red solid line means a cut in the part, the dashed black line separates the left and right sides of dimples.

a) *logitudal cuts*   b) *transversal cuts*
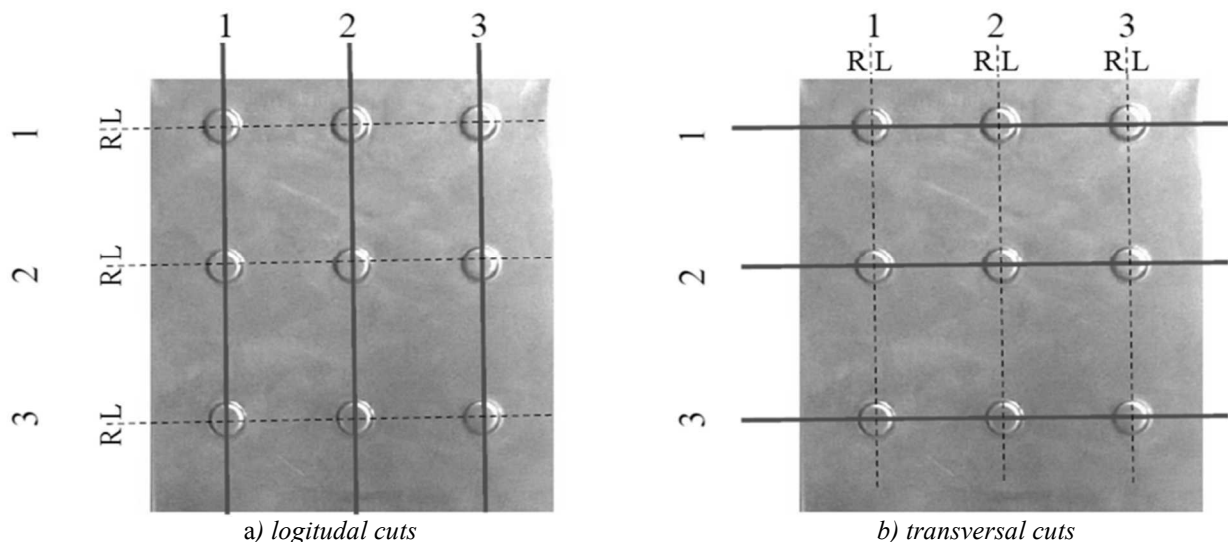
**Fig. 3** *Cutting Sections on Stamped Parts*

In each cut, for the given dimple, the place with the greatest thinning was found by the microscopic measurement, see an example of the thinning evaluation in Fig. 4. The largest thinning was found at the fillet location at the bottom of each dimple.

From the measured data, the average values were calculated for individual rows and columns. Left and right sides of each cut dimple were also distinguished in order to observe the effect of the punch and the die displacement. In both longitudinal and transverse cuts, the right and left side thinning values differ in approx. 0.009 mm. Therefore, the utilization of a perfectly coaxial tool could mean a maximum increase in thickness by 3 % in relation to the initial thickness of the blank s = 0.3 mm.
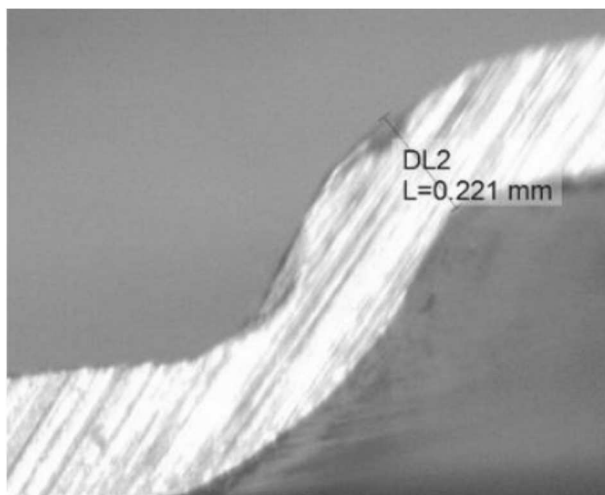
a) left side of the dimple
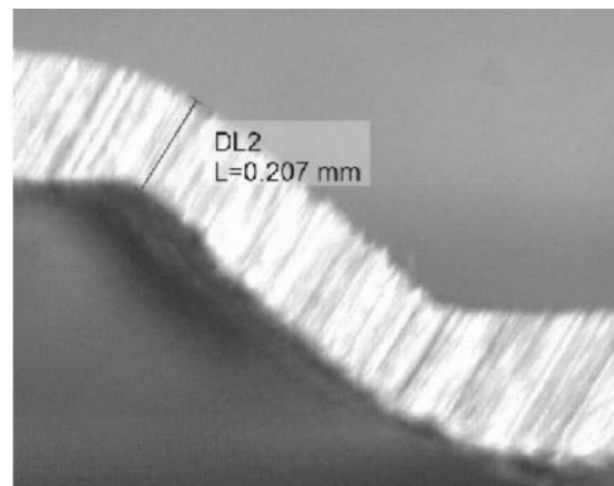

b) right side of the dimple

Fig. 4 *Example of Measured Dimple*

Tab. 5 *Thickness Values for Longitudal Cuts in mm*

		Column 1	Column 2	Column 3	Mean value
Row 1	Right side	0.178	0.174	0.177	0.176
	Left side	0.202	0.193	0.201	0.199
Row 2	Right side	0.156	0.192	0.199	0.182
	Left side	0.189	0.188	0.202	0.193
Row 3	Right side	0.196	0.192	0.205	0.198
	Left side	0.212	0.202	0.200	0.205
Summary mean value	Right sides				0.185
	Left sides				0.199
	Overall longitudinal mean value				0.192

Tab. 6 *Thickness Values for Transversal Cuts in mm*

	Column 1		Column 2		Column 3	
	Left side	Right side	Left side	Right side	Left side	Right side
Row 1	0.212	0.192	0.177	0.195	0.190	0.202
Row 2	0.189	0.196	0.211	0.199	0.205	0.204
Row 3	0.229	0.206	0.221	0.207	0.262	0.209
Mean value	0.210	0.198	0.203	0.200	0.219	0.205
Summary mean value	Right sides					0.201
	Left sides					0.211
	Overall transversal mean value					0.206

3 Geometry Optimization by Using Numerical Simulation
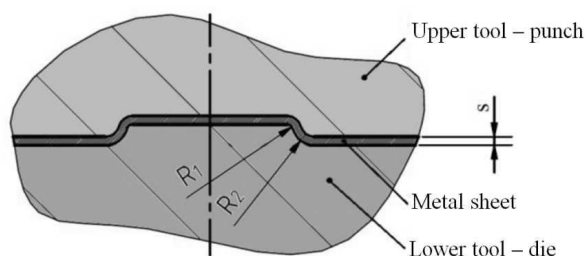
Fig. 3 *Geometry of Stamped Dimple [3]*

The aim of the optimization is to choose from various forming tools shapes combinations such that the thinning of the stamped dimples wall at the radii of R_1 and R_2 is as small as possible (Fig. 3). The dimple must still simultaneously have an acceptable shape due to its function of the spacer element. In the initial condition, the dimple geometry consists of fillet radii of $R_1 = 0.2$ mm, $R_2 = 0.8$ mm and initial sheet thickness s = 0.3 mm. In addition, the thinning will be evaluated for three different materials, X2CrCuTi18 ferritic steel, X5CrNi18-10 austenitic steel and X5CrNi18-10 austenitic steel with additional heat treatment.

The dimple geometry is determined primarily by the size of the radii R_1 and R_2. If the size of these radii changes, the strain and stress will change during the stamping process, as well as the final thickness of the dimple wall. For this purpose, a numerical simulation with the support of the finite element method, that can serve to analyze a wide range of forming analyzes [7], [8], [9], appears to be a highly effective tool. In this case, the choice of the ideal R_1 and R_2 combination, depending on the size of the thinning (or the principal strain), was performed by using an optimization tool in the ANSYS Workbench software. Since the ANSYS software does not allow a thickness

change evaluation, the thinning value has to be determined by recalculating the the principal strain over the thickness using equation (1).
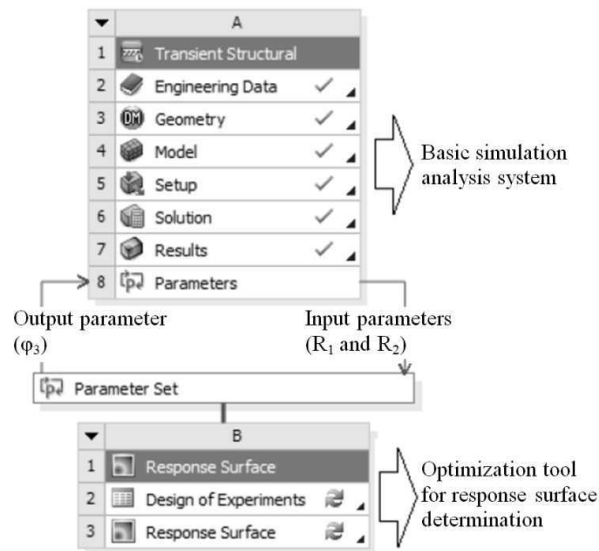
$$s = s_0 \cdot e^{\varphi_3} \text{ [mm]}, \tag{1}$$

Where:

s...Actual thickness [mm],

s_0...Initial thickness (0.3 mm) [mm],

φ_3...True principal strain over the thickness [-].

Fig. 4 Basic Schema of the Project in ANSYS Workbench Software [3]

The mentioned tool uses the response surface method, which searches for the corresponding output variables according to several input parameters. [10] Based on their interdependence, an optimal combination of input parameters is then sought. Fig. 4 shows a solution schema in ANSYS Workbench. Due to the parameterization of the whole model, the geometry change, based on input parameters, could be controlled by a program that calculated

a minimal strain value φ_3 for each combination and thus a minimal dimple thickness.

3.1 Geometric model

The geometry description is based on the CAD data, which were provided by Hanon Systems. For the sheet forming simulations using FEM, it is preferable to use shell elements for discretization, that was also used in this case. The geometric model for the detail of one dimple after discretization is shown in Fig. 5. The stamping tools were considered as ideal rigid.
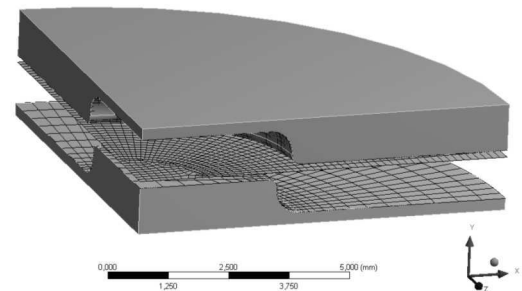
Fig. 5 Discretization in FEM Model [3]

3.2 Material model

For above-mentioned three materials, tensile tests were performed in the rolling direction. Thus obtained engineering stress-strain curves (hardening curves) were subsequently converted into true values. A comparison of the detected curves after recalculation (from the yield stress to the ultimate strength of each material) to true stress–strain values is given in Graph 1. Together with elastic properties (Tab. 2 and Tab. 4) and other simulation parameters (i. e. friction coefficient, which was determined as $\mu = 0,12$), recalculated true values can be used as a material model for FEM simulations. Moreover, normal anisotropy coefficients were also identified for the anisotropic behavior of the materials, see Tab. 5.
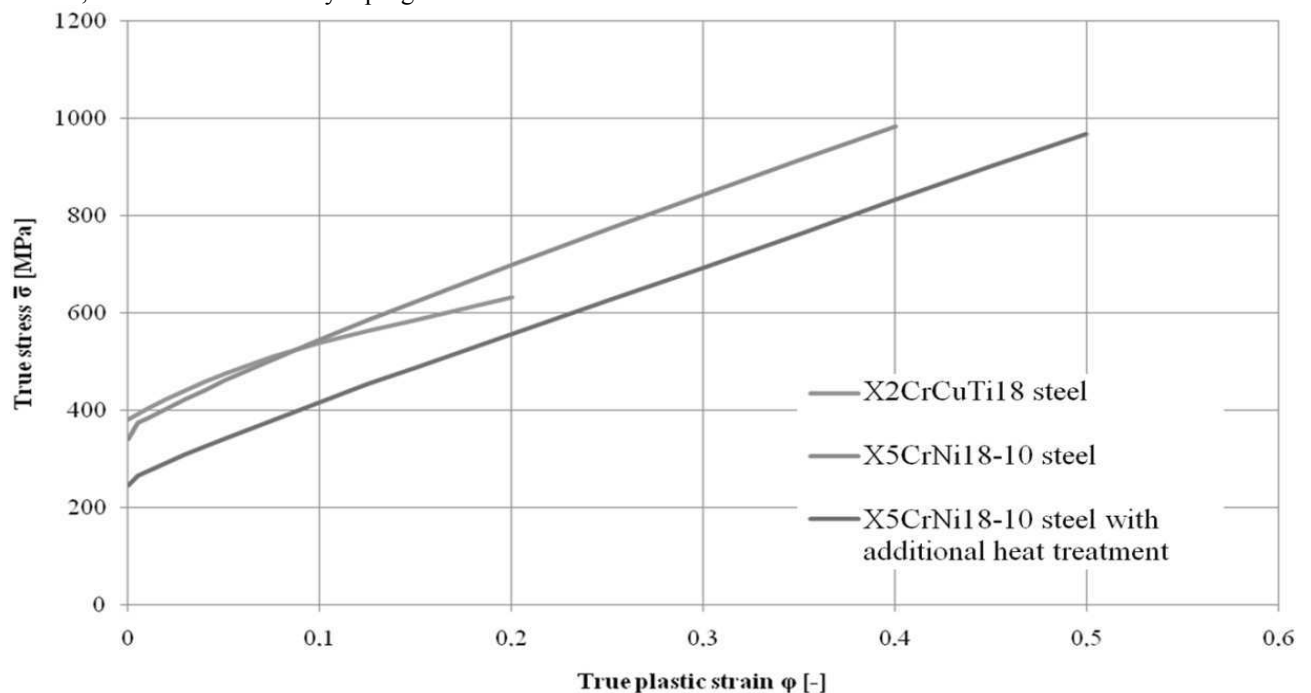

Graph 1 True Stress-Strain Curves of Solved Materials

Tab. 5 *Normal Anisotropy Coefficients of Solved Materials*

|	X2CrCuTi18 steel	X5CrNi18-10 steel	X5CrNi18-10 steel with additional annealing
$r_{0°}$	1.291	0.865	0.902
$r_{45°}$	0.831	1.174	1.087
$r_{90°}$	1.198	0.972	0.815
r_s	1.038	1.046	0.973

3.3 Simulation Results

Due to its strength characteristics, ferritic stainless steel X2CrCuTi18 shows the worst values of thinning in comparison with austenitic sheets, as expected. A sample of the third principal strain distribution (over the thickness) in the direction of the sheet thickness after the stamping process is shown in Fig. 6.


a) Detail for One Dimple　　　　　*b) Overall View of the Stamped Part*
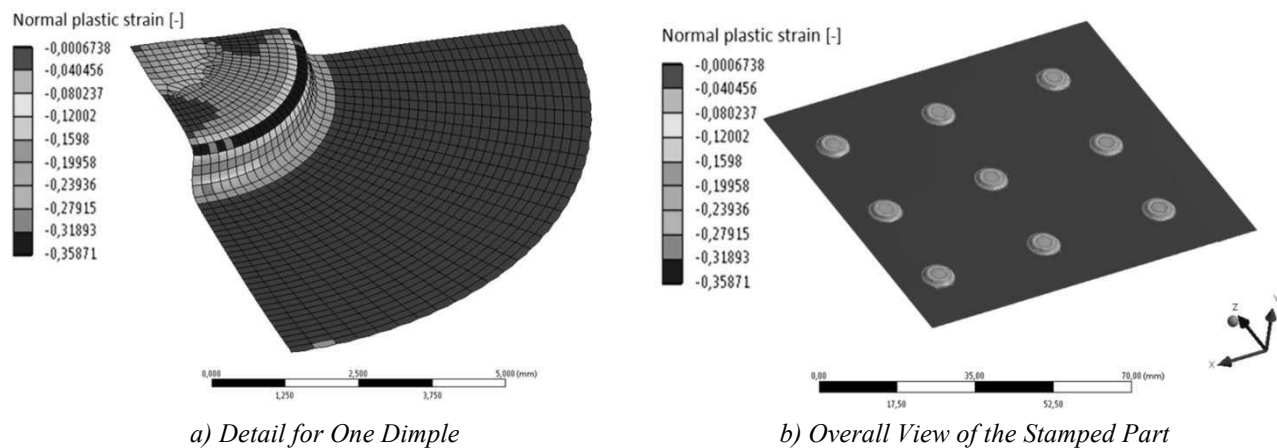
**Fig. 6** *Third Principal Strain Distrimution After Stamping*

This is the result for the combination of R1 = 0.2 mm and R2 = 0.5 mm, i. e. current state. After the recalculation according equation (1), the lowest strain corresponds to a thickness of 0.222 mm (25.9% thinning). The response surface for the other R_1 and R_2 values is shown in Graph 2. As it is logically evident from the mentioned diagram, the wall thinning is decreasing along with the increasing radii R_1 and R_2.
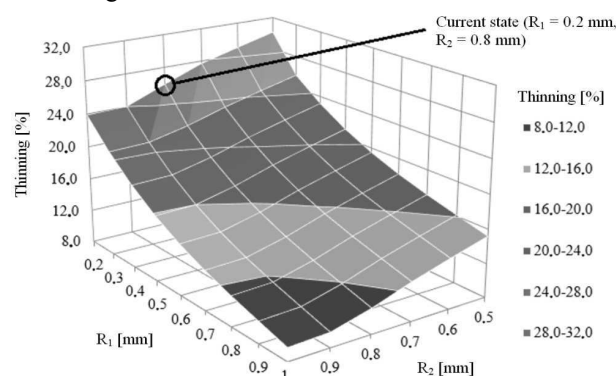
Graph 2 *Dependency of Wall Thinning on R_1 and R_2 for X2CrCuTi18 Steel*

For verification of the accuracy of numerical simulation results, it is also necessary to compare the FEM simulation of the current state with the above-mentioned experimental thickness measurement. By simulating the current state, a minimum thickness of 0.222 mm was found at a critical point (near R_1 radius), corresponding to the thinning value of 25.9 %. By microscopical measuring, 33.3% thinning was found as the largest value, i. e.

difference of 7.4 %. It is important to note, that the difference can be affected by many factors, such as changes in friction coefficient, but namely by relative displacement of stamping tools toward each other in practical manufacturing process etc. In view of the foregoing, the model can be regarded as sufficient to search the optimal geometry parameters, a radius R_1 and R_2. Austenitic stainless steel X5CrNi18-10 without additional heat treatment confirmed the expected reduction in thinning values. As in the previous case, the dependence of thinning on input simulation parameters (R_1 and R_2) can be observed in Graph 3. Unlike steel, it is possible to achieve a smaller thinning. For the current state, minimal thining value of 23.8 % was found.
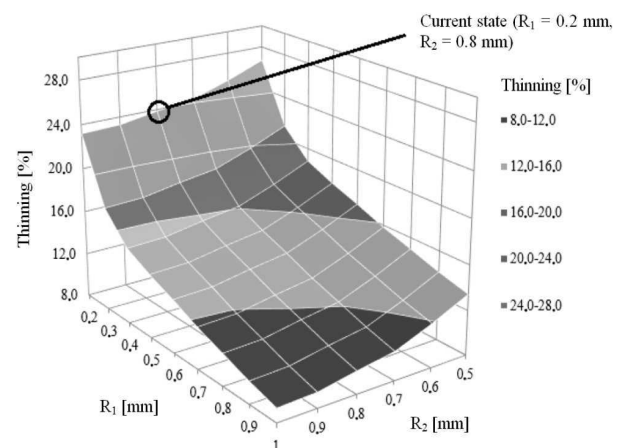
Graph 3 *Dependency of Wall Thinning on R_1 and R_2 for X5CrNi18-10 Steel*
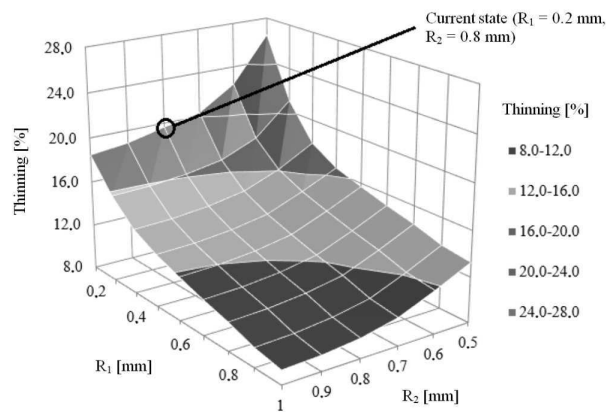
Graph 4 *Dependency of Wall Thinning on R_1 and R_2 for X5CrNi18-10 Steel with Additional Heat Treatment*

The third and final material variant is austenitic stainless steel X5CrNi18-10 with additional heat treatment. By changing of the main geometric parameters (R_1 and R_2), a graph of the dependence between percentage thinning of the material, R_1 radius and R_2 radius was also for this third case constructed, see Graph 4. For the

current state, the lowest thinning value was found as 19.6%, which is the best result for all three cases. As in the two previous cases, it is also possible to state, that the radius R_1 has more impact on thinning values, compared to R_2 influence.

4 Results and Discussion

As it follows from the above-mentioned, X5CrNi18-10 steel with additional heat treatment seems to be the most advantageous. The graphs presented above show the thinning depending on the dimple geometry. However, attention should also be paid to the materials influence across these graphs. The comparison of thinning values shows that the greatest influence of the material properties appears for the small radii R_2 and namely R_1. By increasing of these parameters the material's influence is reduced. This is illustrated in Graph 5a, where the thinning curves for all three materials can be seen, depending on R_1 at $R_2 = 0.6$ mm. Furthermore, Graph 5b shows another case, i. e. the same dependence for $R_2 = 1$ mm. Curves characterizing the thinning are approaching with increasing values of radii R_1 and R_2.
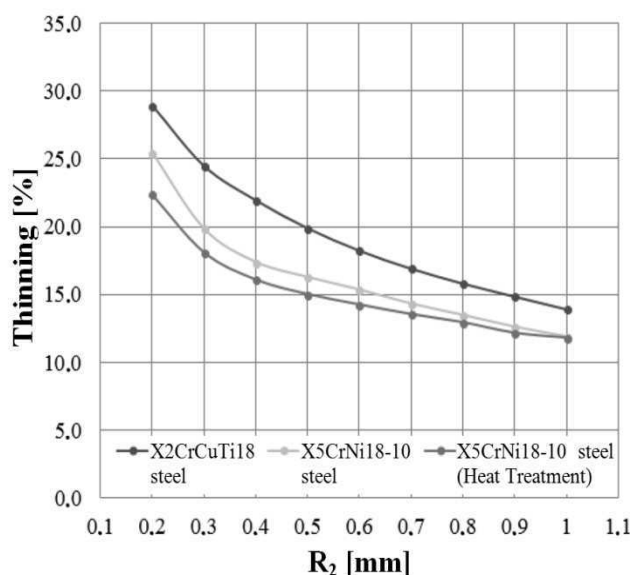
a) for $R_2 = 0,6$ mm
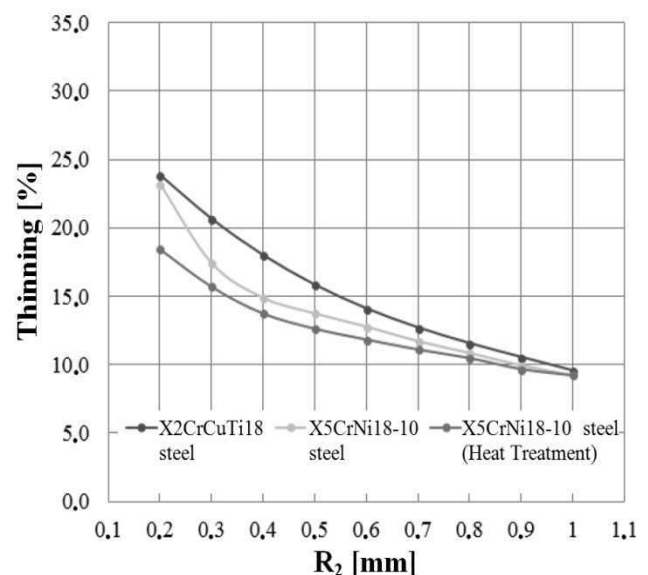
b) for $R_2 = 1$ mm

Graph 5 *Effect of Material and R_1 Radius on Thinning*

There are several paths to reach the lower wall thinning. The first way is to increase both radii to values as close as possible to the maximum in a tested range. In this case, it is not important what type of considered materials will be used, because for $R_1 = R_2 = 1.0$ mm, the difference in the thinning is in the order of tenths of a percent. Therefore, it makes no sense to use a more expensive material option. In other hands, the dimple function as a spacer element defining the position of the entire part with respect to the whole assembly may be in conflict with its shape change. For this reason, if it is not possible to change the geometry to the recommended one, the second way how to increase the dimple wall thickness is just changing of the blank material.

5 Conclusions

The article was focused on the design of the dimple geometry depending on its thinning. In this case, the determination of material thinning during the stamping operation was performed by using numerical analysis, i.e. finite element method. Overall, three types of blank materials were analyzed (ferritic steel, austenitic steel and austenitic steel with additional heat treatment) with initial thickness of 0.3 mm. Before the mentioned analysis, mechanical behavior of all analyzed materials was evaluated by performing the tensile test. In the following, experimental evaluation of thinning was done by using microscopic measurement on the current geometry.

The theoretical analysis showed that the current state (ferritic steel, $R_1 = 0.2$ mm, $R_2 = 0.8$ mm) cannot be stamped with less thinning than approx. 26 %, varying from the minimal experimentally determined value by 7.4%. If the tool geometry is changed to $R_1 = 1$ mm, $R_2 = 1$ mm, the thinning value reaches the lower value of 9.55 %. When austenitic steel is using, it is possible to achieve even lower values for the same geometry, namely 9.24 %. But austenitic steel with additional heat treatment (annealing) achieves the best thinning values (thinning of 9.23 % for R_1, $R_2 = 1$ mm). It is obvious that the use of austenitic steel with additional heat treatment can positively affect the thinning of the material, up to 0.32 %. In all cases, it can be observed that the change in rounding value R_1 brings a steeper course of thinning change, compared to R_2. Therefore it is obvious that the effect of the radius R_1 is more pronounced for all investigated cases.

Acknowledgement

References

[1] KUMAR, V., QUATTAWI, A. (2018). Nusselt Number and Friction Factor Correlations of Three Sides Concave Dimple Roughened Solar Air Heater. In: *Renewable Energy*, Vol. 12, No. 2, pp. 355 – 377. Elsevier. United Kingdom.

[2] HOSFORD, W. F., CADDEL, R. M. (2014). *Metal forming: Mechanics and metallurgy*. Cambridge University Press, United Kingdom.

[3] FALTÝNEK, L. (2018). *Geometry Optimization of the Stamped Part*. Brno University of Technology. Czech Republic.

[4] PTÁČEK, L. (2002). *Nauka o materiálu II.* CERM. Brno.

[5] ČSN EN 10088-1. (2015) Stainless Steel - Part 1: Overview of Stainless Steels. pp. 1–80. Czech Standards Institute. Prague.

[6] ŘIHÁČEK, J. (2018). *Utilization of Hydroforming Hechnology to Create a Structured Surface of Solar Panel.* Brno University of Technology. Czech Republic.

[7] PETERKOVÁ, E. (2016). Biaxial Test of Tubes Using Elastomer. In: *Manufacturing technology*. Vol. 16, No. 4, pp.765–771. J. E. Purkyne University. Czech Republic.

[8] ŽMINDÁK, M., MEŠKO, J., PELAGIĆ, Z., ZRAK, A. (2014). *Finite element analysis of crack growth in pipelines*. In: *Manufacturing Technology*. Vol. 14, No. 1, pp. 116-122. J. E. Purkyne University. Czech Republic..

[9] ALBAT, M., QUATTAWI, A. (2017). Numerical Simulation of Sheet Metal Forming: a Review. In: *The International Journal of Advanced Manufacturing Technology*, Vol. 89, No. 1, pp. 1235 – 1250. Springer. United Kingdom.

[10] LEE, H.-H. (2017). *Finite Element Simulations with ANSYS Workbench 17: Theory, Applications, Case Studies*. SDC Publishing, United States.